

# Numerical Investigation of the Shape Memory Alloy Dowels in Jointed Concrete Pavements

Saeid Hesami<sup>1</sup> and Vahid Sadeghi<sup>1+</sup>

**Abstract:** Shape memory alloy (SMA) is a novel functional material, which has found increasing applications in different engineering aspects. This research presents a finite element analysis of the potential benefits of SMA dowel bars on the jointed concrete pavements (JCP). With a 3-dimensional (3D) Finite element modelling (FEM) and application of the damaged plasticity model, the tensile damage around the three types of SMA dowels are calculated, and the results are compared to conventional steel dowel bars in the JCP. It was found that SMA dowels considerably reduce the damages around the dowels through the concrete slabs. The load transfer efficiency (LTE) of the pavement equipped with these smart dowels are also have been discussed. To gain further understanding of the pavement behavior, a dynamic load was repeated a thousand times on the model. The damage and the LTE under repetitive loads have been investigated, and it is concluded that SMA dowels can maintain their load efficiency even under highly repeated loads, while causing less tensile damages to the pavement.

**DOI:** 10.6135/ijprt.org.tw/2015.8(4).251

**Key words:** Concrete damaged plasticity; Dowel bar; Finite element; Load transfer efficiency; Shape memory alloy.

## Introduction

JCPs are mostly used for the roads due to their good performance. Inclusion of dowel bars at transverse joints in the JCPs is necessary to transfer the traffic loads applied on a slab to an adjacent slab and it enhances the structural capacity at the joints. It also prevents faulting and pumping in JCPs. The deterioration of the concrete around the dowels has adverse effects on the dowel load transferring performance. In the present study, a 3D FE model was established for analyzing a dowel-jointed concrete pavement, equipped with smart dowels. The 3D model was verified with an existing experimental test in the literature.

Three-Dimensional Finite Element modeling (3D-FEM) has been widely used to investigate the dowel bars at joints in rigid pavements by various researchers. Byrum used a calibrated FEM model to numerically evaluate the joint load transfer [1]. Levi developed a 3D-FE model to investigate a typical joint system with misaligned dowels and determined local damage of concrete with utilizing ABAQUS program [2]. The state of maximum stresses generated around the dowel bars was also investigated by various researchers showing that concrete degradation around dowels adversely affects dowel performance [3]. Shoukry et al. showed that radial strain in concrete around the dowel is not uniform along the dowel circumference. With application of FEM he also showed that the magnitudes of stresses in concrete surrounding uncoated steel dowels are comparatively high [4] FEM and experimental studies by Riad et al. indicated the existence of compressive stresses at the top and bottom of the dowel, and the more critical tensile stresses at both sides of the dowel bar at the concrete-dowel interface. Tensile cracks and damage happened when tensile stresses exceeded the

tensile strength [5]. Ioannides utilized ABAQUS FEM program to simulate crack propagation in concrete pavement with application of Hillerborg Crack model [6]. Shortcomings of dowels have been remarked in various studies. Steel dowels are corroded by the presence of water and salt which leads to the higher internal stresses due to expansion. This phenomenon causes the concrete to crack and spall. There is an extensive literature review regarding application of various dowel types but the corrosion susceptibility remains a critical issue for these bars [7]. Repeated wheel load causes the concrete around the dowels to deteriorate, which adversely affects the load transfer efficiency of the dowel between the adjacent slabs [8]. Whereas literature shows that SMAs are highly durable and corrosion resistance materials compared to steel, hence they can improve the surrounded concrete structure [9-11].

The objective of this study is to propose a new dowel system based on SMAs to reduce the concrete damage around the dowel bars. In present work shape memory effect properties of Nitinol, Iron and copper based Shape Memory alloy (SMA) dowel bars behavior compared to the conventional steel dowels under loading are investigated through detailed 3D FEM using ABAQUS. The damaged plasticity model for concrete is used in order to carry out the static and dynamic nonlinear analysis of concrete pavement. The load transfer efficiency (LTE) of the mentioned alloys and steel dowels were analyzed under single and repetitive wheel loads.

## Shape Memory Alloys

SMA are unique alloys that are able to undergo large deformation and recover to its predetermined shape by unloading or heating. The unique ability to revert to initial shape upon heating is called shape memory effect (SME). The phenomenon that SMA can undergo inelastic deformation and recover their initial shape after unloading is called superelasticity (pseudoelasticity). SMA has two crystal (Atomic) structures. Stronger Austenite phase is stable in high temperature, and the weaker Martensite phase is stable in lower

<sup>1</sup> Babol University of Technology, Babol, Iran.

<sup>+</sup> Corresponding Author: E-mail sadeghi@stu.nit.ac.ir

Note: Submitted December 6, 2014; Revised April 21, 2015;

Accepted May 29, 2015.

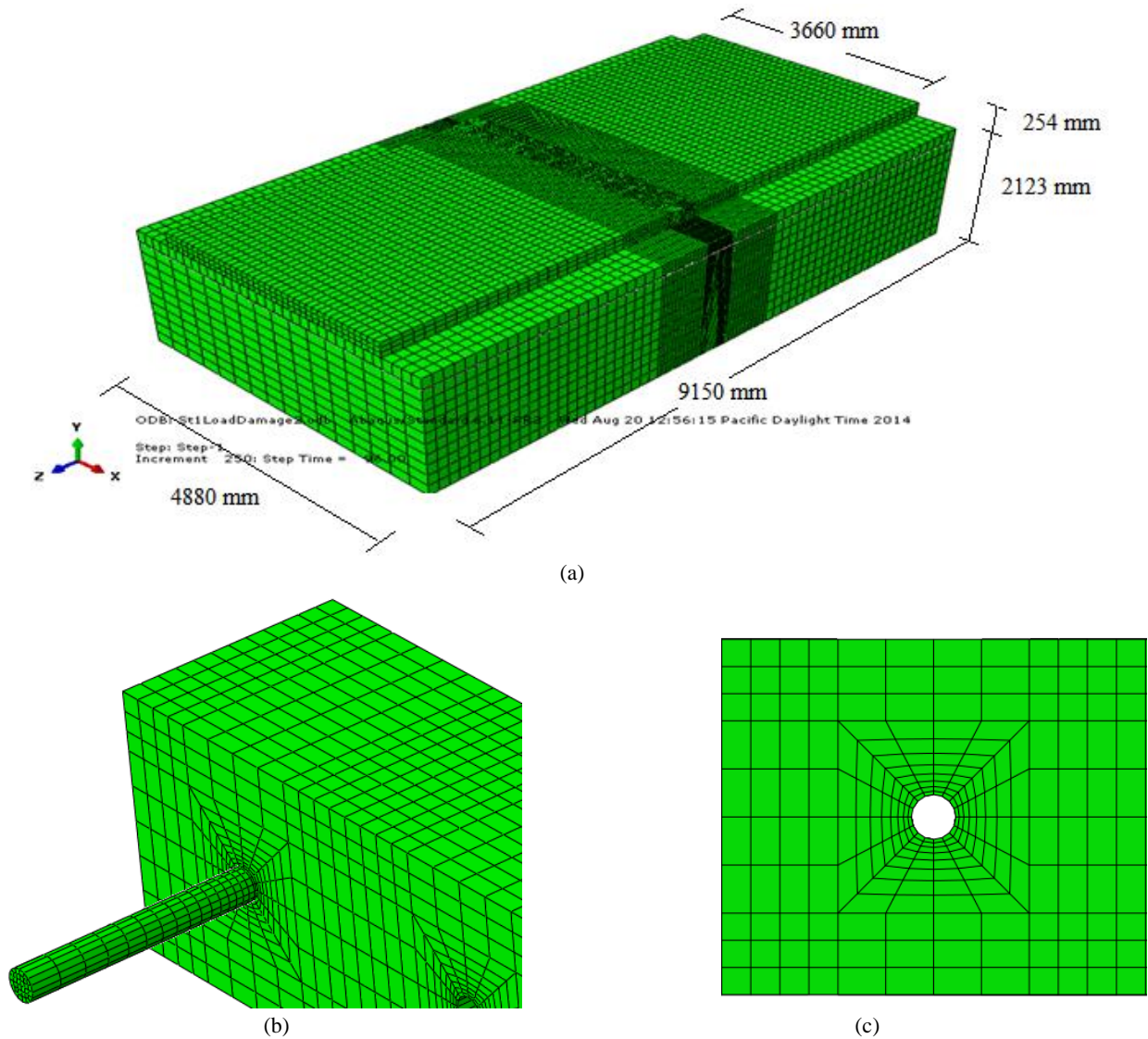


**Fig. 1.** Finite Element Mesh Used in the Study.

temperature [9]. The predominant structure depends on temperature and stress which cause peculiar characteristics to SMA. Structure in the austenite state transforms to the Martensite state when it is loaded above a certain stress level. Upon unloading the Martensite is no longer stable and a back transformation to Austenite occurs [10, 12]. Many alloys displaying the SME have been found, not all are suited to industrial manufacturing because of the high price. Nitinol (NiTi) and copper based alloys have much higher strength and larger recoverable strain and excellent corrosion resistance compared to other alloys. Iron based SMAs have been largely studied and improved during the last years. The lower cost of the Fe–Mn–Si-based alloys compared to the conventional SMAs makes it more favorable for practical use of Iron based SMAs as the structural material. Iron based alloys can be modified to gain a very high recovery stress and become corrosion resistance [13, 14]. SMAs have been widely used in civil engineering and other fields and industries in past 30 years. The comprehensive understanding and control of their surprising behavior are still being developed [15-17]. A few researches have been conducted to investigate the usage of SMAs in road and transportation industry for expansion

joints. These expansion joint showed excellent behavior during earthquakes and thermal loads [18, 19]. The superior fatigue behavior of this material can be interesting for engineering fields including pavement engineering. Within elastic regime SMA can have a fatigue life as high as 107 cycles [12]. Here in this study SMA are used as a dowel bars in JPC. The properties of the shape memory alloys are shown in Table 1, which have been defined in Software as user implemented material.

### Model Description

A two-slab system separated by a 10-mm joint sitting on top of supporting layers was modeled using ABAQUS program. Solid 3D Element was used to model the concrete pavement. The model geometry is similar to the model presented by Shoukry et al [20]. Regarding that the stress under the wheel load was anticipated to be less than the strength of concrete, a linear elastic constitutive model were used for the concrete slab and the underneath layers. The 254 mm thick slabs were 4600 mm long and 3660 mm wide, with a modulus of elasticity  $E = 29000$  MPa, a Poisson's ratio  $\nu$  of

**Table 1.** Shape Memory Effect Mechanical Properties.

Alloy	Cu-Al-Ni	Ni-Ti	Fe-Mn-Si
Density (gr/cm <sup>3</sup> )	7.12	6.45	7.45
Elasticity Modulus (Austenite) (GPa)	85	70	170
Elasticity Modulus (Martensite) (GPa)	80	30	130
Ultimate Tensile Strength (MPa)	500-800	895-1900	680-1,000
Recovery Strain (%)	4%	8%	4.50%
Poisson Ratio	0.343	0.33	0.359

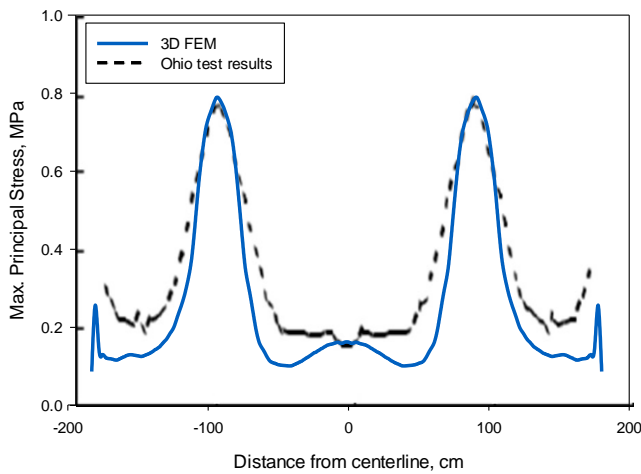


**Fig. 2.** Model Verification.

0.22 and a density of 2400 kg/m<sup>3</sup>. The transverse joint had twelve 32 mm diameter, 470 mm long dowels, spaced at 300 mm on center. Frictional contact stress is considered between the slab and base layer. A refined mesh zone was located at the center of the joint, where wheel loads are applied, as illustrated in Fig. 1. Fig. 1(a), 1(b), and 1(c) illustrates the finite element mesh for the dowel used in this research. A base layer of 200 mm thick ( $E = 310 \text{ MPa}$  and  $\nu = 0.3$ ) was modelled on top of the subgrade with  $E = 30 \text{ MPa}$  and  $\nu = 0.45$ . A bonded interface action was considered between subgrade and base and their width were increased to reduce side boundary condition effect on slab response.

**Model Loading**

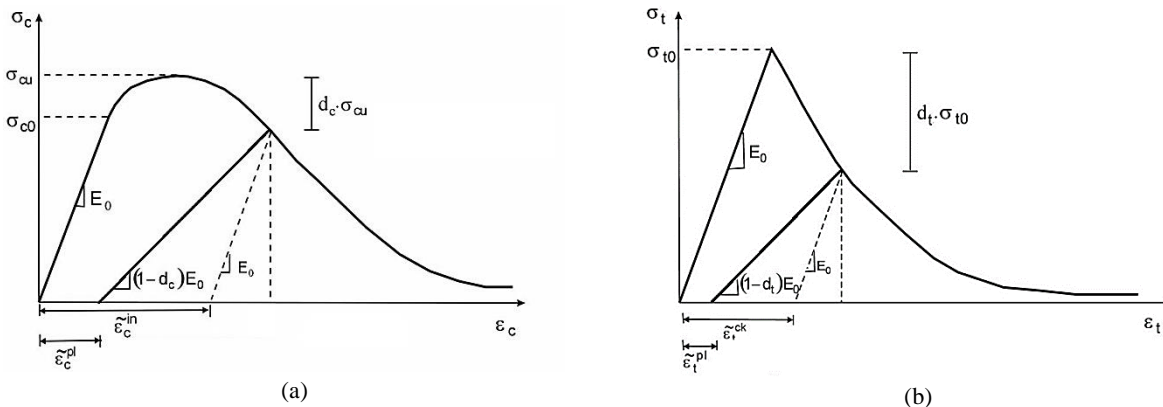


**Fig. 3.** Dependence  $\sigma - \epsilon$  in Compression (a) and Tension (b) for CDP Model.

The model is loaded under single axle configuration. A single axle load consisting of two 80 kN load is selected for this study. Spacing between the wheels is approximately 1800 mm. The contact area is a rectangular shape with 300 mm length and 230 mm width. To investigate the maximum damage induced around the dowels, wheels must be in the most critical location, so the loads are applied directly on joints. To simulate the surrounding damage and dowel's LTE under repeated moving loads, the axle load is moved on the joint, 1000 times.

**Model Validation**

To verify the accuracy of the theoretical model, its result is measured with the result of a field study in the Ohio State [21]. The Max principal stress along the wheel path, at 76 mm away from the joint, obtained from the model is compared to Ohio Test Road result. The comparison between the predicted and experimental results shows a very good agreement (Fig. 2).

**Concrete Damage Plasticity**

The formation of microcracks in concrete is represented macroscopically as strain-softening behavior of the material, causing tensile cracking, compressive failure and a complete loss of strength [22, 23]. The concrete damage plasticity model is provided in ABAQUS for capturing the effects of irreversible damage associated with the failure mechanisms. The degradation of the elastic stiffness is characterized by two tensile and compressive damage variables,  $d_t$  and  $d_c$  which are assumed to be functions of the plastic strains, temperature, and field variables. The damage variables can take values from zero, for the undamaged material, to one, which represents total loss of strength. Stress – cracking strain ( $\tilde{\epsilon}_t^{ck}$ ) in uniaxial tension and stress – crushing strain ( $\tilde{\epsilon}_c^{in}$ ) and their dependence in uniaxial compression can be defined. Fig. 3 shows, which values in CDP model are interpreted as the cracking strain and the crushing strain.

In Fig. 3  $\sigma_{c0}$  and  $\sigma_{cu}$  are the compressive stress point in which nonlinear behavior initiates and the ultimate compressive strength of the concrete respectively.  $\sigma_{t0}$  is the ultimate tensile stress point in which non-linear behavior begins. After reaching the maximum

stress, the stiffness of the concrete during unloading decreases. The rate of stiffness reduction is related to the damage of the concrete and can be determined from the multiplication of initial stiffness ( $E_0$ ) to  $1-d_t$  or  $1-d_c$ . The resulting strains followed by a reduced stiffness in zero stress point are plastic compressive strain ( $\epsilon_c^{pl}$ ) and plastic tensile strain ( $\epsilon_t^{pl}$ ) and can be calculated by Eqs. (1) to (2) [22, 23].

$$\epsilon_c^{pl} = \epsilon_c^{in} - \frac{d_c \cdot \sigma_c}{(1-d_c) \cdot E_0} \tag{1}$$

$$\epsilon_t^{pl} = \epsilon_t^{ck} - \frac{d_t \cdot \sigma_t}{(1-d_t) \cdot E_0} \tag{2}$$

In these equations  $\sigma_c$  and  $\sigma_t$  are compressive and tensile strength in any points after the maximum stress. Before the maximum stress in stress-strain chart the damage is considered equal to zero. The damage after the maximum stress can be calculated from Eqs. (3) to (4).

$$d_c = \frac{\sigma_{cu} - \sigma_c}{\sigma_{cu}} \tag{3}$$

$$d_t = \frac{\sigma_{tu} - \sigma_t}{\sigma_{tu}} \tag{4}$$

This study aims to reduce tensile concrete damage with using SMA dowels in JCP.

### Model Results

Load applied on the first slab is transferred to the adjacent slab through dowel bars. During this transmission, the concrete around the dowels is damaged. The damage in the first slab under the load is higher. The concrete damage around the dowels in the first slab is illustrated in Fig. 4. Around 2 centimeters of the concrete around the dowels is highly damaged, but except for the four dowels under the wheel load, the damage gradually diminishes along the dowels. These four dowels (dowels No. 3, 4, 8, 9) which are located under the wheel load, caused concrete to damage about 10 cm along the dowel. SMA dowel has a significant effect on reducing these damages.

From Fig. 4(a) it can be understood that the concrete mostly deteriorated when steel dowels are utilized. The least damage is caused by Nitinol dowels (Fig. 4(d)). Fig. 4(b) and 4(c) shows that copper and Iron based dowels have a better performance than steel dowel bar. Tensile damage of the concrete around the dowel is different for each scenario. When steel dowel is used, damage for the 6 cm of the concrete around the dowels No 3 and No 4 are 0.69 and 0.61 respectively. In case of iron based dowels these damages are computed 0.54 and 0.46, 0.38 and 0.3 for copper based dowels and 0.25 and 0.16 for Nitinol dowels. The average damage to the concrete around dowels for each case is given in Table 2.

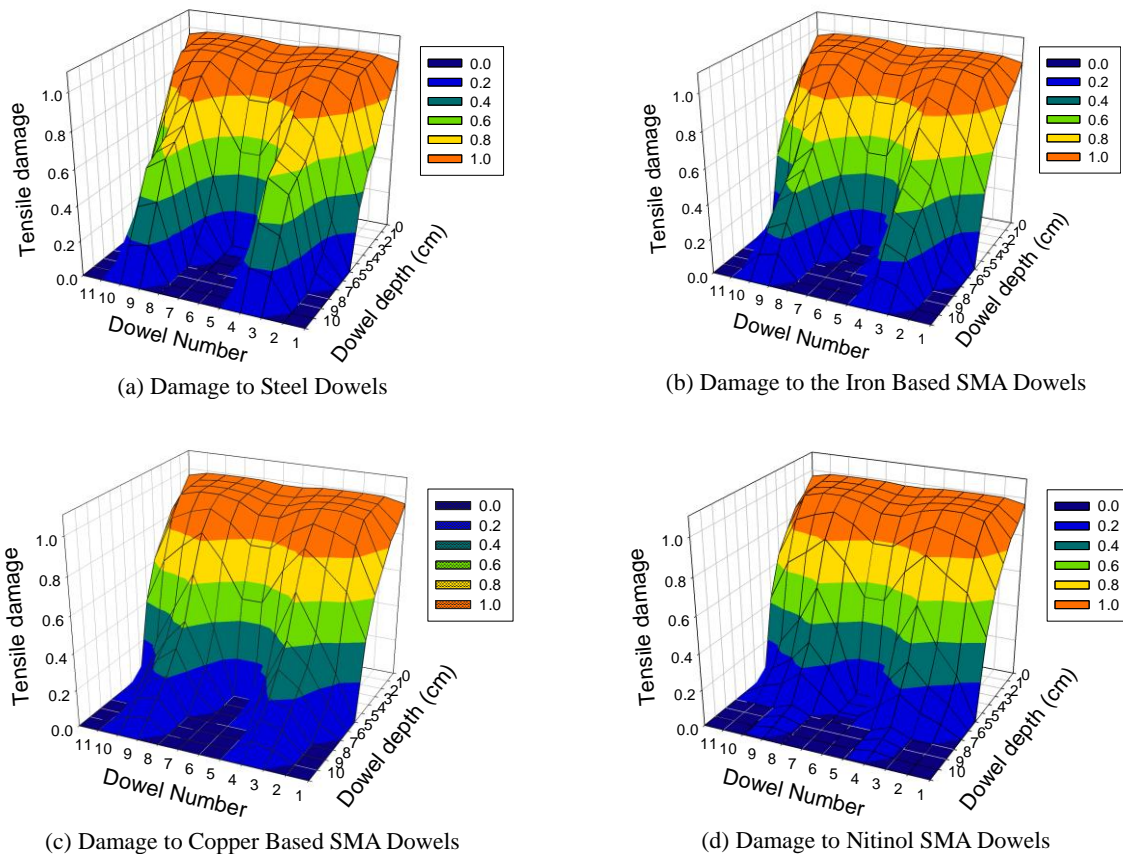


Fig. 4. Tensile Damage the Concrete Around the Dowels.

**Table 2.** The Average Damage to the Dowels.

Dowel Type	Steel		Iron (SMA)		Copper (SMA)		NiTi (SMA)	
Dowel No.	3	4	3	4	3	4	3	4
Avg. Damage	0.84	0.94	0.78	0.89	0.71	0.82	0.66	0.77

**Table 3.** LTE of the Studied Dowels under Single Axle Load

Dowel Type	Steel Dowels	Iron Based Dowels	Copper Based Dowels	NiTi Dowels
Average LTE	0.974	0.971	0.967	0.959
LTE Under Wheel Load	0.955	0.952	0.946	0.941

From the Table 2, it can be concluded that the Nitinol decreased the tensile damage more than iron and copper based dowels. Nitinol has a 7000 MPa modulus of elasticity. The copper has 8500 MPa modulus of elasticity. The lower the modulus of elasticity is the damage is less, however lower moduli of elasticity compromises the load transfer between the two slabs.

The joint load transfer efficiency for each dowel type under single passage of axle load is given in the Table 3. It can be observed that the iron based SMA dowel has the highest load transfer efficiency compared to other alloys. The load transfer efficiency is defined by Eq. (5):

$$LTE = \frac{\Delta_u}{\Delta_l} \quad (5)$$

where  $\Delta_u$  and  $\Delta_l$  are deflection of the unloaded and loaded side of the slab.

LTE is critical in dowels exactly beneath the wheel loads, the lowest LTE belongs to NiTi dowel. The average LTE is calculated by determining LTE under each dowel.

From the Table 3 it can be observed that, clearly for a single passage of load with a very low speed (almost static) the LTE of all dowels are within acceptable range. Average LTE indicates the mean LTE for all dowels, the critical LTE is obtained under the wheel load and it is calculated separately. The critical LTEs of all dowels are within the acceptable range.

To gain further insights into the behavior of the joints under repeated load, the effects of a thousand single axial loads passage was simulated. The wheel loads are moved on the joint with the speed of 30 km/hr. Fig. 5 displays the damage to concrete around the dowels 3 and 4, which have been found most critical dowels before, under 50, 100, 200, 400, 600, 800, and 1000 wheel load

passages for each dowel type.

Fig. 5 shows that the about 10.5 cm of the concrete surrounding the steel dowel, after the 1000th passage of the wheel load, is mostly damaged, which is 1.5 times more than iron based SMA dowel, 1.9 times more than copper and 2.1 times more than Nitinol. The average damage to the concrete around the dowels No. 3 and No. 4 are given in the Tables 4 and 5 respectively.

The results show that SMA reduced the maximum damage to the concrete along the dowels. The damage was less in higher loading cycles. Nitinol reduced the damage more than other dowels. The performances of the other alloys were better than the steel dowel in higher cycles.

Fig. 6 presents the loss of LTE during repetitive loadings. In initial cycles when the damage to the dowels slightly increases, the LTE will gradually decrease. In higher cycles as the magnitude of damage to the concrete surrounding the dowels increases the rate of LTE loss will also increase. So clearly, LTE of the dowels and damage are related to each other. The charts reveal that SMA dowels has a significant effect on the LTE during life of the pavements.

It is very important to mention that Shape memory materials can return to their original shape by heating, after the plastic deformation under the passing loads. Regarding to this characteristic, a special system can be built in which dowels are heated by the electrical resistance heating, after they are deformed. This can help restoring LTE to its high primary values.

## Conclusion

This paper has examined SMA dowel bars as a replacement for conventional steel dowel bar in typical concrete pavements numerically. The study employed a detailed FEM model developed

**Table 4.** Average Damage to the Concrete Around the Dowel No. 3 in All Cases.

Passage	50	100	200	400	600	800	1000
Steel Dowel	0.17	0.25	0.32	0.38	0.45	0.52	0.58
Iron (SMA)	0.16	0.23	0.29	0.34	0.41	0.46	0.51
Copper (SMA)	0.15	0.23	0.26	0.31	0.36	0.40	0.45
Nitinol (SMA)	0.15	0.22	0.25	0.29	0.34	0.37	0.41

**Table 5.** Average Damage to the Concrete Around the Dowel No. 4 in All Cases.

Passage	50	100	200	400	600	800	1000
Steel Dowel	0.19	0.28	0.35	0.42	0.48	0.54	0.61
Iron (SMA)	0.18	0.26	0.32	0.37	0.43	0.48	0.54
Copper (SMA)	0.17	0.25	0.30	0.35	0.40	0.44	0.50
Nitinol (SMA)	0.17	0.24	0.28	0.32	0.37	0.41	0.45

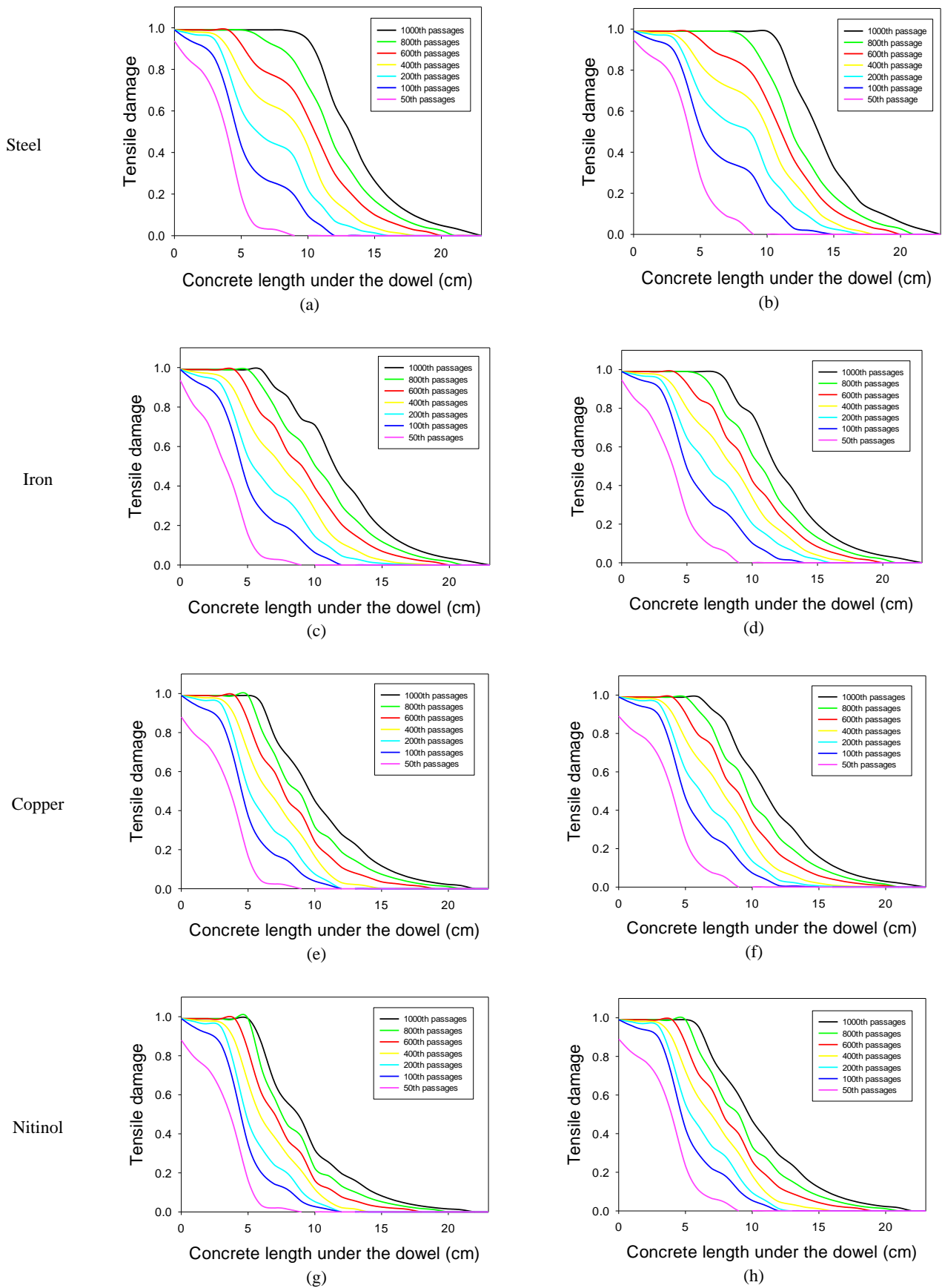
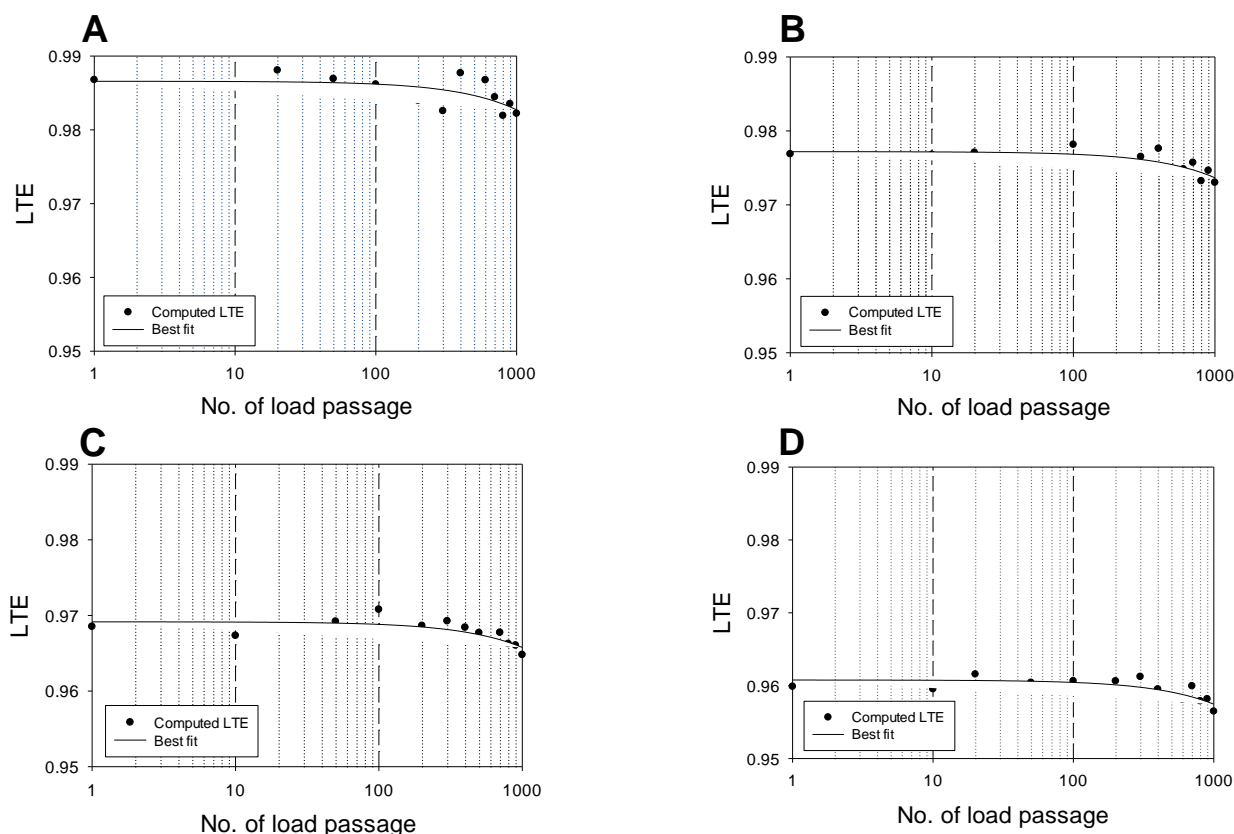


Fig. 5. Tensile Damage Around the Dowels No. 3 (a, c, e and g) and 4 (b, d, f and g).



**Fig. 6.** LTE versus No. of Load Passages for A: Steel Dowels, B: Iron Based SMA Dowels, C: Copper Based SMA Dowels and D: Nitinol Dowel.

with ABAQUS. After validating the pavement model, several models with utilizing different SMA dowels, including Nitinol, copper and Iron based alloys were developed to assess the effectiveness of these smart materials in reduction of the damage to the concrete surrounding the dowels. By application of the damage plasticity model, the damage to the concrete around the each shape memory dowel is determined and compared to conventional steel dowels. The load transfer efficiency of the critical dowels under the wheel load and the mean LTE for all dowels are calculated.

The results of the study have shown that the application of SMA dowels have a significant effect on the damage around the dowels, especially the dowels exactly under the wheel loads.

SMA dowels significantly decrease the damage around the dowels within the JCPs. Joints if equipped with SMA dowels, perform better under repetitive loads. The damage to the surrounding concrete of SMA dowels will be much less, And LTE will be well preserved under the repetitive loads compared to the steel dowels, in other words the loss of the load transfer efficiency of the joints equipped with SMA will be much less than the conventional steel dowels.

## References

- Byrum, C.R. and Ye, D. (2012). Evaluating the effect of concrete slab curling on joint load transfer responses. *Transportation Research Record*, No. 2305(1), pp. 43-53.
- Levy, C. (2010). Numerical Investigation of the Effects of Shrinkage and Thermal Loading on the Behaviour of Misaligned Dowels in Jointed Concrete Pavement. Master of Applied Science thesis, *Waterloo, Ontario, Canada*.
- Davids, W.G., Wang, Z., Turkiyyah, G., Mahoney, J.P., and Bush, D. (2003). Three-dimensional finite element analysis of jointed plain concrete pavement with EverFE2. 2. *Transportation Research Record*, No. 1853(1), pp. 92-99.
- Shoukry, S.N., William, G.W., and Riad, M.Y. (2003). Effect of Bonding Force on Stresses in Concrete Slabs. *West Virginia Department of Transportation*, West Virginia, USA.
- Riad, M.Y. (2001). Stress concentration around dowel bars in jointed rigid concrete pavements, *M.S Thesis*, West Virginia University, Morgantown, West Virginia, USA.
- Ioannides, A.M., Peng, J., and Swindler, Jr, J.R. (2006). ABAQUS model for PCC slab cracking. *International Journal of Pavement Engineering*, 7(4), pp. 311-321.
- Abo-Qudais, S.A. and Al-Qadi, I.L. (2000). Dowel bars corrosion in concrete pavement. *Canadian Journal of Civil Engineering*, 27(6), pp. 1240-1247.
- Maitra, S.R., Reddy, K., and Ramachandra, L. (2009). Load transfer characteristics of dowel bar system in jointed concrete pavement. *Journal of Transportation Engineering*, 135(11), pp. 813-821.
- Lexcellent, C. (2013). *Shape-Memory Alloys Handbook*. John Wiley & Sons, Hoboken, New Jersey, USA.
- Yamauchi, K., Ohkata, I., Tsuchiya, K., and Miyazaki, S. (2011). *Shape memory and superelastic alloys: Applications and technologies*. Woodhead Publishing Limited, Sawston, Cambridge, UK.

11. Cismasiu, C. (2010). Shape memory alloys. Sciyo, Rijeka, Croatia.
12. Lagoudas, D.C. (2008). Shape memory alloys. Springer, New York, USA.
13. Cladera, A., Weber, B., Leinenbach, C., Czaderski, C., Shahverdi, M., and Motavalli, M. (2014). Iron-based shape memory alloys for civil engineering structures: An overview. *Construction and Building Materials*, 63, pp. 281-293.
14. Czaderski, C., Shahverdi, M., Bronnimann, R., Leinenbach, C., and Motavalli, M. (2014). Feasibility of iron-based shape memory alloy strips for prestressed strengthening of concrete structures, *Construction and Building Materials*, 56, pp. 94-105.
15. Song, G., Ma, N., and Li, H.N. (2006). Applications of shape memory alloys in civil structures. *Engineering Structures*, 28(9), pp. 1266-1274.
16. Janke, L., Czaderski, C., Motavalli, M., and Ruth, J. (2005). Applications of shape memory alloys in civil engineering structures--Overview, limits and new ideas. *Materials and Structures*, 38(5), pp. 578-592.
17. Alam, M., Youssef, M., and Nehdi, M. (2007). Utilizing shape memory alloys to enhance the performance and safety of civil infrastructure: a review. *Canadian Journal of Civil Engineering*, 34(9), pp. 1075-1086.
18. DesRoches, R. (2002). Application of shape memory alloys in seismic rehabilitation of bridges. *Technical Report NCHRP-IDEA Project 65*, Transportation Research Board, Washington, DC, USA.
19. Padgett, J.E. and DesRoches, R. (2013). Shape Memory Alloy Enhanced SMART Expansion Joints, Final Report for *NCHRP IDEA Project 147*, National Cooperative Highway Research Program, Transportation Research Board, Washington, DC, USA.
20. Shoukry, S.N., William, G., and Riad, M. (2002). Characteristics of concrete contact stresses in doweled transverse joints. *International Journal of Pavement Engineering*, 3(2), pp. 117-129.
21. Shoukry, S., William, G., and Srinivasan, S. (2002). Analysis of mid-slab transverse cracking in jointed concrete pavements. *International Journal of Pavements*, 1(3), pp. 81-94.
22. Lee, J. and Fenves, G.L. (1998). Plastic-damage model for cyclic loading of concrete structures. *Journal of Engineering Mechanics*, 124(8), pp. 892-900.
23. Lubliner, J., Oliver, J., Oller, S., and Onate, E. (1989). A plastic-damage model for concrete. *International Journal of Solids and Structures*, 25(3), pp. 299-326.